– SUPPORTING INFORMATION –

Organic Super-reducing Photocatalysts Generate Solvated Electrons via Two Consecutive Photon Induced Processes

Marco Villa, Andrea Fermi, Francesco Calogero, Xia Wu, Andrea Gualandi, Pier Giorgio Cozzi, Alessandro Troisi, Barbara Ventura, Paola Ceroni

Table of contents

SYNTHETIC PROCEDURES

Materials and general procedures. All chemicals were purchased from Merck KGaA while solvents from ACS and were used without further purifications. Water was purified by reverse osmometry with an Elga Purelab Classic purification system (18.2 MΩ·cm). The ^{1}H-NMR spectra were recorded at 298 K in CD_3CN or $CDCl_3$ with a Varian Mercury 400 MHz. Chemical shifts were calibrated using the internal residual signal for each used solvent ($CDCl_3$ = 7.26 ppm; CD_3CN = 1.94 ppm). All chemical shifts are quoted using the δ scale (in ppm) and all coupling constants (J) are expressed in Hertz (Hz).

Synthesis of 2,4,5,6-tetrakis(diphenylamino)-isophthalonitrile (4DPAIPN)

A modified literature procedure was adopted for the synthesis of **4DPAIPN**.[1,2] Under Nitrogen atmosphere, a 50 mL heat-gun dried two-necked round-bottom flask was filled with dry DMF (10 mL) and diphenylamine (5.6 mmol, 948 mg, 6 equiv.) under inert atmosphere. NaH (60% suspension in mineral oil, 7.5 mmol, 300 mg, 8 eq.) was slowly added and the mixture was stirred at 50 °C for 5 hours. 2,4,5,6-tetrafluoroisophthalonitrile (0.9 mmol, 187 mg, 1 equiv.) was added and the reaction mixture was stirred at 90 °C for 8 hours. After that, the solution was cooled to 0°C and water (1 mL) was slowly added to quench the reaction. A yellow precipitate appeared upon addition of MeOH (10 mL) and was collected by filtration. The solid was redissolved in DCM (10 mL) and reprecipitated by the addition of MeOH (10 mL) to afford the desired clean product (Yield: 60%, 0.54 mmol, 431 mg). Spectroscopic data are in agreement with those reported in literature.[1]

Synthesis of f 2,4,5,6-tetrakis(carbazol-9-yl)-4,6-dicyanobenzene (4CZIPN)

A modified literature procedure was adopted for the synthesis of **4CzIPN**.[3,4] Under Nitrogen atmosphere, a 50 mL two-necked round-bottom-flask, equipped with a magnetic stirring bar, was charged with carbazole (5.0 equiv., 10 mmol, 1.67 g) and dry THF (20 mL). The solution was cooled down to 0 °C and NaH (60% in mineral oil, 7.5 equiv., 15 mmol, 600 mg) was slowly added under vigorous stirring. After 2 hours, tetrafluoroisophthalonitrile (1.0 equiv., 2 mmol, 400 mg) was added and the mixture was stirred at room temperature overnight. A yellow precipitate progressively appeared. When the TLC showed a complete conversion of the starting material, water (1 mL) was added dropwise under vigorous stirring to neutralize the excess of NaH, and the mixture was evaporated to give a yellow solid. The solid was successively washed with water and ethanol to afford 1.09 g (1.38 mmol, 69% yield) of spectroscopically pure 4CzIPN. Spectroscopic data are in agreement with those reported in literature.

Synthesis of bis(tetrabutylammonium)oxalate (TBAOx)

A modified literature procedure was adopted for the synthesis of **TBAOx**.[5] Under Argon atmosphere, a 25 mL two-necked round-bottom-flask, equipped with a magnetic stirring bar, was charged with oxalic acid dihydrate (1.0 equiv., 5 mmol, 630 mg). At room temperature Tetra-*n*-butylammonium hydroxide, 40% w/w in methanol (2.0 equiv., 10mmol, 7.1 mL) was added dropwise. The solution was allowed to stir until disappearance of oxalic acid dihydrate was observed. After 2 h of stirring, the solvent was removed under reduced yielding first a gelatinous material and then a white powder. The desired TBAOx was obtained in quantitative yield (> 95%, 2.8 g). Spectroscopic data are in agreement with those reported in literature.[5]

PHOTOPHYSICAL CHARACTERIZATION

Photophysical measurements. Optically diluted solutions with concentrations in the order of 10^{-4} or 10^{-6} M were prepared in spectroscopic or HPLC grade solvents for steady-state and time-resolved absorption and emission analysis. Absorption spectra were recorded at room temperature on a Varian Cary 50 spectrophotometer with 1 cm or 0.2 cm quartz cuvettes. Degassed solutions were prepared via 4 consecutive freeze-pump-thaw cycles and spectra were taken using home-made Schlenk quartz cuvette; alternatively, N_2-saturated solutions were prepared in a glove box using the same glassware. Steady-state emission, excitation spectra and time-resolved emission spectra were recorded at 298 K using an Edinburgh Instruments F920 or a Edinburgh Instruments FS5, equipped with a Hamamatsu R928 phototube. Samples were excited at 390 nm for steady-state measurements and at 340 or 405 nm for time-resolved measurements. For emission lifetimes < 10 μs the above-mentioned Edinburgh Instruments F920 fluorometer, equipped with a time-correlated single-photon counting (TCSPC) module was used. For the determination of excited state lifetimes through TCSPC, emission decays were fitted with single or multiple exponential functions; the associated χ^2 values ($1 < \chi^2 < 2$) were determined using the EI FS5 or Edinburgh FLS920 software. The estimated experimental errors are 2 nm on the band maximum, 5% on the molar absorption coefficient and luminescence lifetime and 10% on the quantum yield.

Photoinduced generation of radical species. Irradiation of samples for the generation of radical species from **4CzIPN** and **4DPAIPN** in the presence of a sacrificial electron donor (DIPEA or TBAOx) in CH_3CN were performed at room temperature on thoroughly stirred N_2-saturated solutions by using a Kessil lamp at 390 nm (40 W). Immediately after irradiation (10-30 s) the so-obtained solutions have been employed for further spectroscopic characterization and analysis.

For the 390-nm Kessil lamp (light power of 400 mW/cm^2), we estimated a photon flux of ca. 1 x 10^{-6} moles of photons/s, so that a 30 s irradiation time corresponds to 3 x 10^{-5} moles of photons. For a solution with absorbance = 0.5 at the irradiation wavelength, the percentage of absorbed light is 68%, corresponding to 2 x 10^{-5} moles of photons, much larger than the moles of photocatalyst in solution (1 x 10^{-7} moles, 2.5 mL of 40 μM solution). Therefore, quantitative generation of the radical anions is feasible under our experimental conditions.

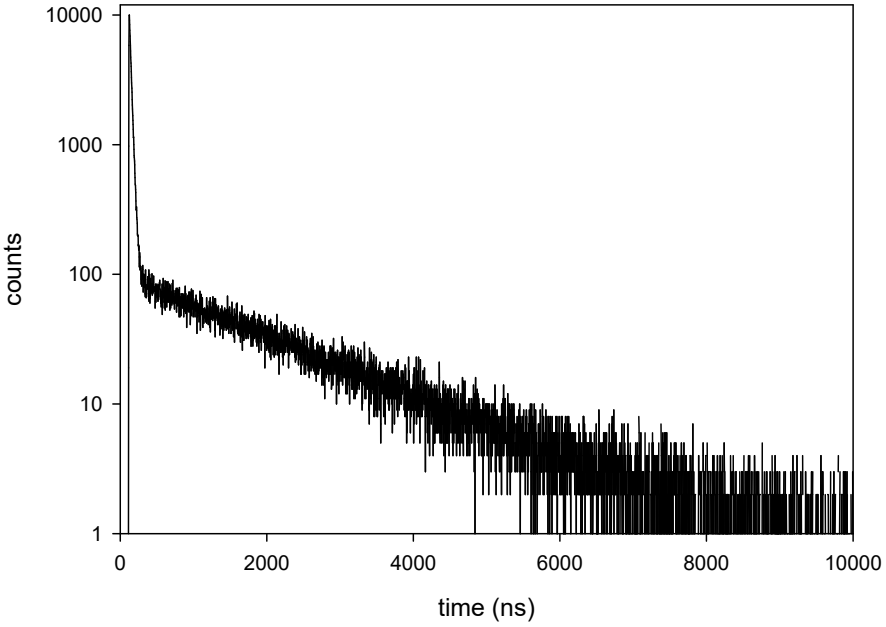

Figure S1. Emission intensity decay of a deareated solution of **4CzIPN** in CH_3CN. λ_{exc} = 405 nm. λ_{em}=550 nm

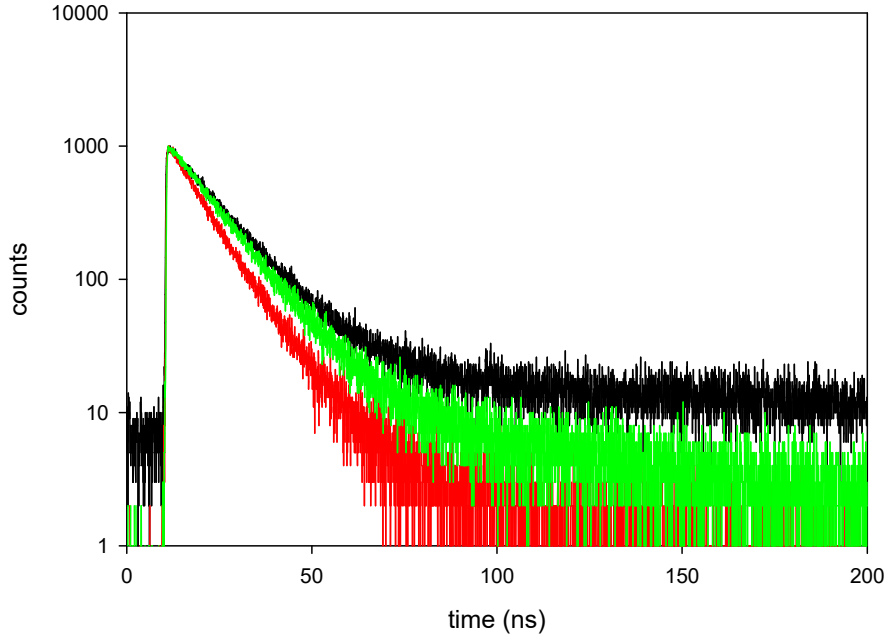

Figure S2. Emission intensity decay of an air-equilibrated solution of **4CzIPN** in CH_3CN (black line) and after addition of DIPEA (10 mM, red line) and TBAOx (5 mM, green line). λ_{exc} = 340 nm, λ_{em} = 550 nm.

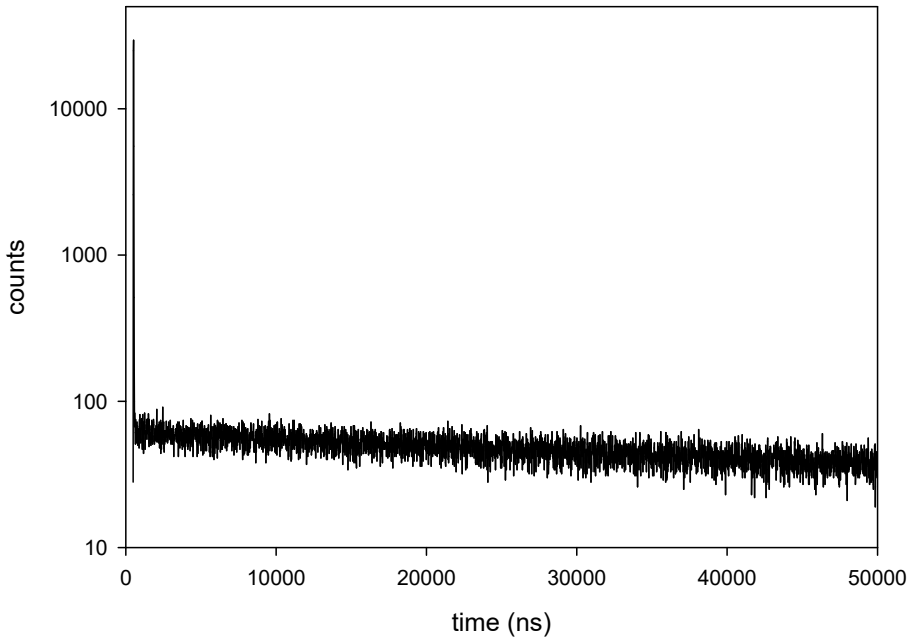

Figure S3. Emission intensity decay of a deareated solution of **4DPAIPN** in CH_3CN. λ_{exc} = 405 nm. λ_{em} = 550 nm.

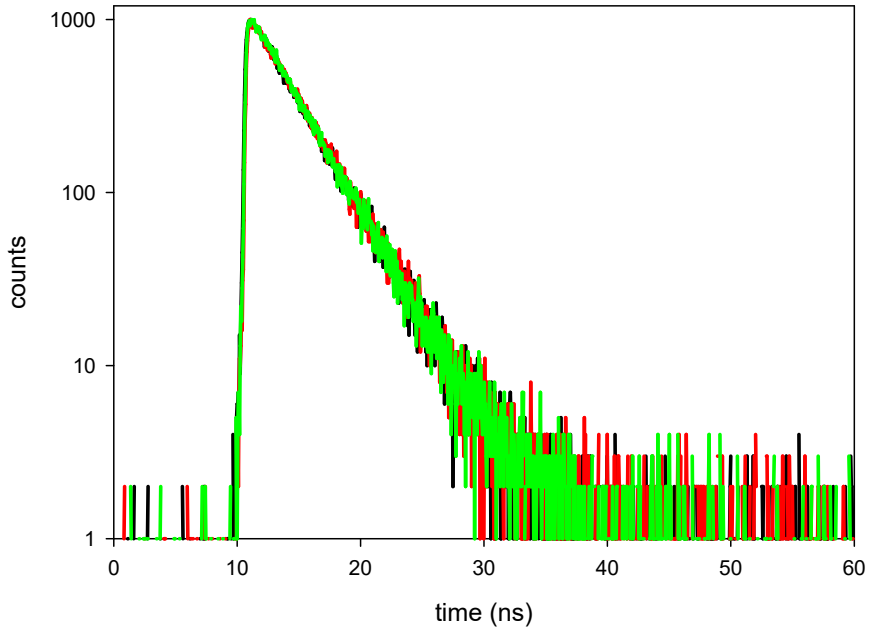

Figure S4. Emission intensity decay of an air-equilibrated solution of **4DPAIPN** in CH_3CN (black line) and after addition of DIPEA (10 mM, red line) and TBAOx (5 mM, green line). λ_{exc} = 340 nm. λ_{em} = 550 nm.

Table S1. Most relevant photophysical parameters for **4CzIPN** and **4DPAIPN** in degassed CH_3CN solution at room temperature with and without TBAOx (5 mM).

	λ_{abs} / nm	λ_{em} / nm	τ^a / ns
4CzIPN	430	545	13.4
4CzIPN + DIPEA	430	545	9.2
4CzIPN + TBAOx	430	545	12.0
4DPAIPN	470	536	3.4
4DPAIPN+ DIPEA	470	536	3.3
4DPAIPN + TBAOx	470	536	3.4

[a]Lifetime of the lowest-energy lying excited state, namely S_1 in the case of **4CzIPN** and **4DPAIPN**.

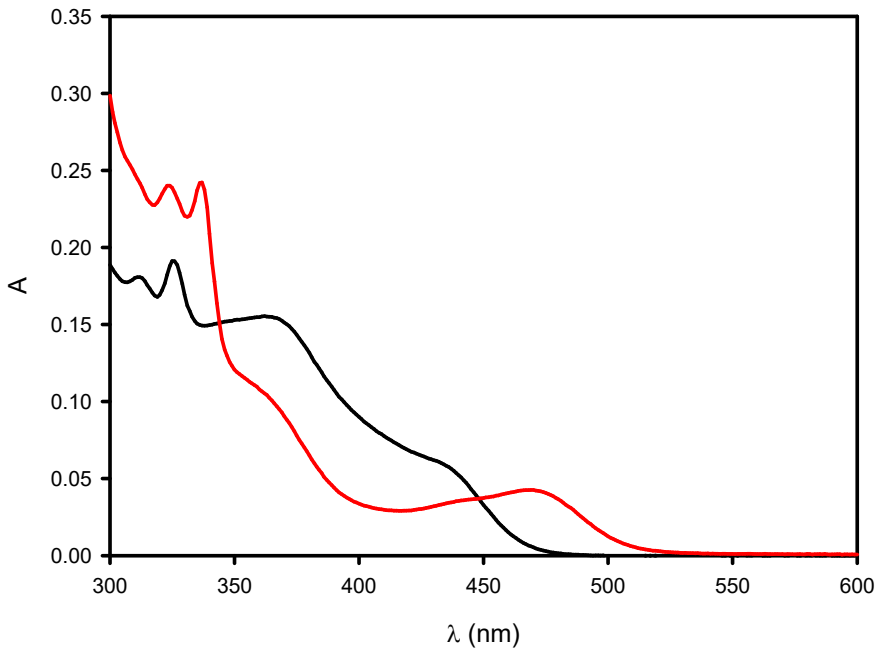

Figure S5. Absorption spectra of a deareated solution of **4CZIPN** in the presence of DIPEA (100 mM) before (black line) and after irradiation at 390 nm (red line).

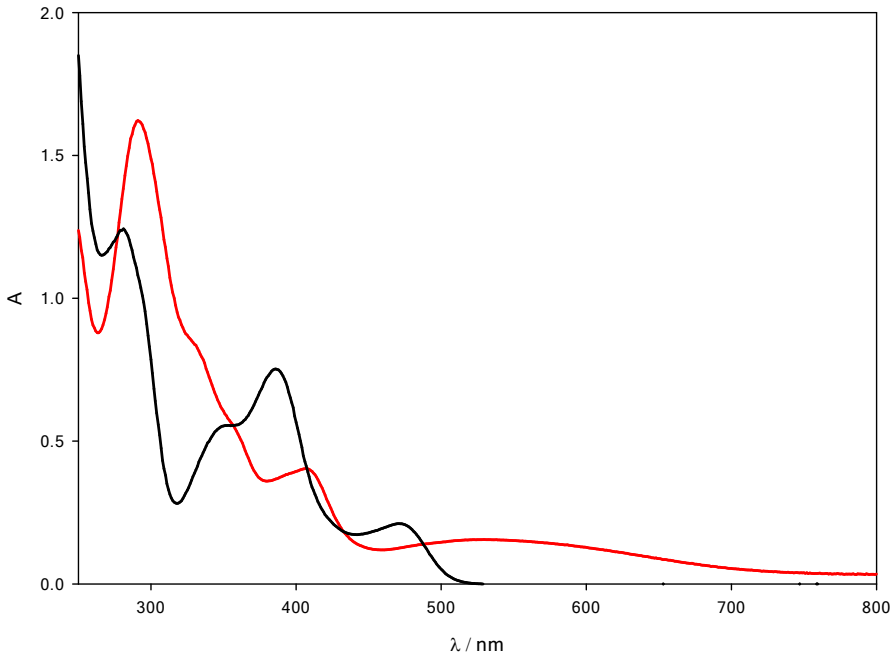

Figure S6. Absorption spectra of a deareated solution of **4DPAIPN** in the presence of DIPEA (100 mM) before (black line) and after irradiation at 390 nm (red line).

TRANSIENT ABSORPTION SPECTROSCOPY

General

Transient absorption in the femtosecond range was performed by means of an Ultrafast Systems HELIOS (HE-VIS-NIR) femtosecond transient absorption spectrometer by using, as an excitation source, a Newport Spectra Physics Solstice-F-1K-230 V laser system, combined with a TOPAS Prime (TPR-TOPAS-F) optical parametric amplifier (pulse width: 100 fs, 1 kHz repetition rate, selected output wavelengths: 390, 480 and 600 nm). The Solstice system was composed of a tunable (690–1040 nm) Mai Tai HP Ti:Sa femtosecond oscillator pumped by a Nd:YVO4 laser (Millennia), a Ti:Sa regenerative amplifier pumped by an intracavity-doubled, Q-switched, diode-pumped Nd:YLF pulsed laser (Empower 30), an optical pulse stretcher, and an optical pulse compressor. The overall temporal resolution of the system is 300 fs. Air-equilibrated solutions in 0.2 cm optical path cells were analyzed under continuous stirring. The pump energy on the sample was 4 μJ/pulse at 390 nm and 8 μJ/pulse at 480 and 600 nm. Surface Xplorer V4 software from Ultrafast Systems was used for the data acquisition and analysis. The 3D data surfaces were corrected for the chirp of the probe pulse prior to the analysis. Lifetimes were taken as average of values derived from the fitting of several decays at different wavelengths. Errors on lifetimes were estimated as average of the errors reported by the fitting software for each lifetime. Steady-state absorption spectra were registered before and after transient absorption experiments to check the photostability of the investigated system.

Transient absorption spectroscopy of 4CzIPN

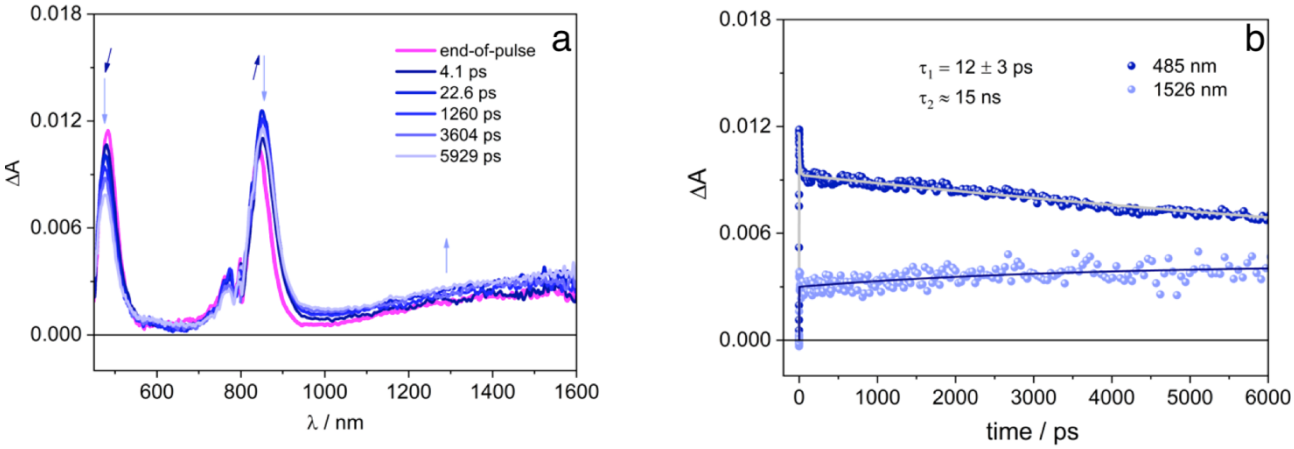

Figure S7. Transient absorption spectra at different delays of **4CzIPN** in acetonitrile solution (a) and the corresponding ΔA temporal evolutions (and fittings, lines) at significant wavelengths (b). λ_{ex} = 390 nm, A_{390} = 0.25, 0.2 cm optical path, 4 μJ/pulse. In (a) the arrows indicate the spectral changes associated with the different processes.

The end-of-pulse spectrum of **4CzIPN** presents two main bands peaked at 484 nm and 847 nm and a broad featureless absorption above 1000 nm (Figure S7a). A first fast process (τ_1 = 12 ps), consistent with internal conversion from upper lying singlet excited states to S_1, as well as solvent rearrangement processes, is observed (decay and few nm blue-shift at 484 nm and rise and few nm red-shift on the 847 nm band). This event is followed by a slow process that exceeds the time window of the experiment (ca. 3 ns) and can be roughly estimated in the order of 15 ns (Figure S7b). This can be attributed to S_1 deactivation, since the lifetime is consistent with that of prompt fluorescence reported in Table S1.

Upon addition of TBAOx (5.2 mM), the transient features of **4CzIPN** are similar: two processes can be identified, with spectral changes consistent with those observed for **4CzIPN** in pure acetonitrile (Figure S8a), and a biexponential temporal evolution with τ_1 = 11 ps and τ_2 ca. 9 ns (Figure S8b). The fast component is very similar to that previously observed, while the long component is shorter, as expected for the quenching of the S_1 excited state of **4CzIPN** in the presence of a 5.2 mM concentration of the sacrificial electron donor (see Table S1).

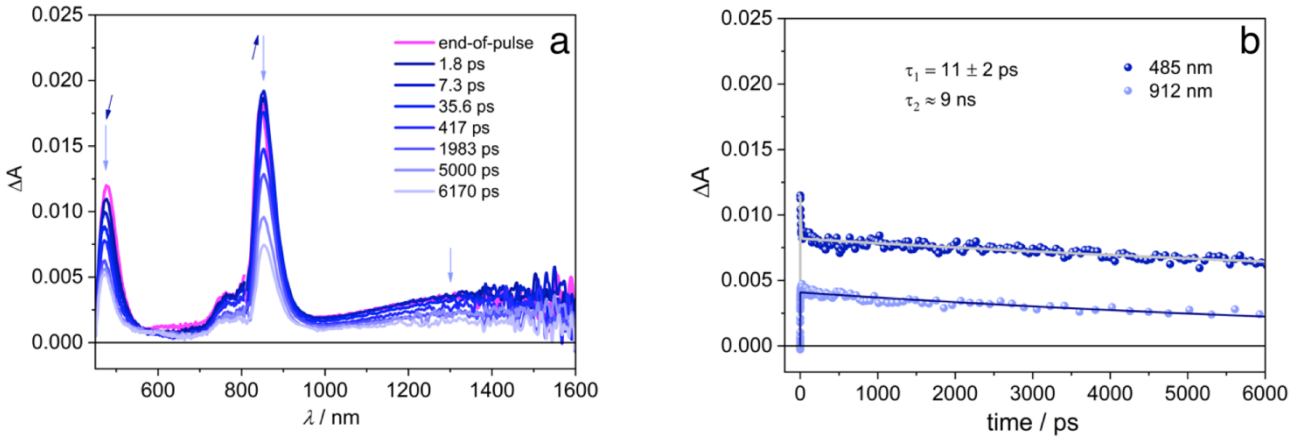

Figure S8. Transient absorption spectra at different delays of **4CzIPN** in acetonitrile solution containing TBAOx (5.2 mM) (a) and the corresponding ΔA temporal evolutions (and fittings, lines) at significant wavelengths (b). λ_{ex} = 390 nm, A_{390} = 0.25, 0.2 cm optical path, 4 μJ/pulse. In (a) the arrows indicate the spectral changes associated with the different processes.

Transient absorption spectroscopy of 4DPAIPN

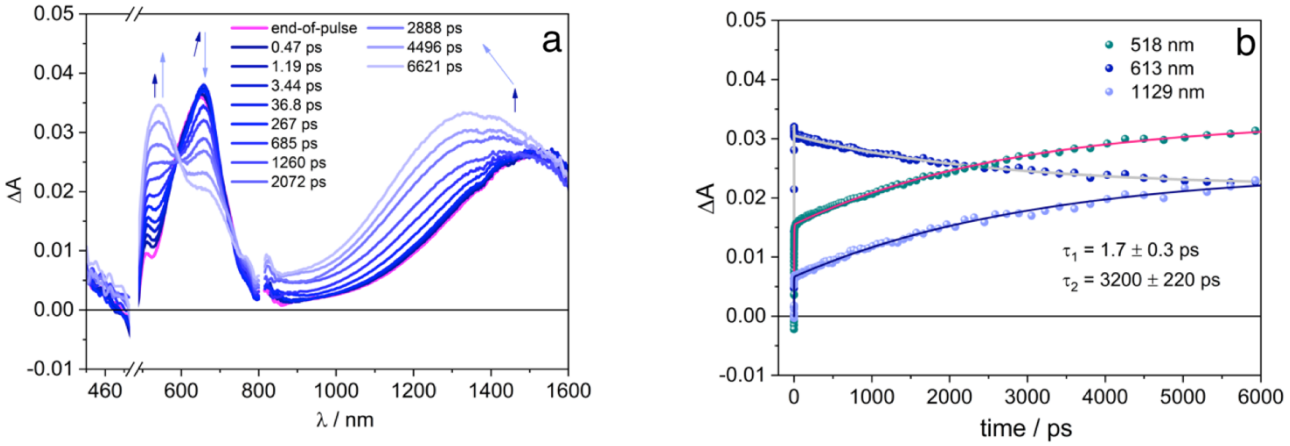

Figure S9. Transient absorption spectra at different delays of **4DPAIPN** in acetonitrile solution (a) and the corresponding ΔA temporal evolution (and fittings, lines) at significant wavelengths (b). λ_{ex} = 480 nm. A_{480} = 0.18, 0.2 cm optical path, 8 μJ/pulse. In (a) the arrows indicate the spectral changes associated with the different processes.

Figure S9a shows the transient absorption features of **4DPAIPN** in acetonitrile solution. An initial spectrum with maxima at 650 nm and 1510 nm evolves towards a signal with blue-shifted bands at 540 nm and 1350 nm. A first fast process of the order of ca. 2 ps is present all over the spectral range, particularly visible on the 650 nm band as a rise and few nm red-shift. The second slow process, leading to the decay of the 650 nm band and to the formation of the bands at 540 nm and 1350 nm, occurs in the order of 3 ns, which corresponds to the lifetime measured for the prompt fluorescence (Table S1). The observed biphasic behavior can hence be ascribed to solvent rearrangement and deactivation of S_1 with concomitant population of T_1. The final spectrum is thus attributed to the T_1 state, which is decaying outside the available time window. It can be noticed that, in the case of **4CzIPN**, the T_1 state population is not clearly visible because the S_1 excited state is longer lived, so that the final spectrum is still dominated by the S_1 features. In presence of TBAOx sacrificial electron donor (5.2 mM), both the spectral and temporal evolutions appear almost identical (Figure S10). The longer lifetime, attributable to S_1 deactivation, is not reduced by the presence of the oxalate, in agreement with the measured prompt fluorescence lifetime (see Table S1).

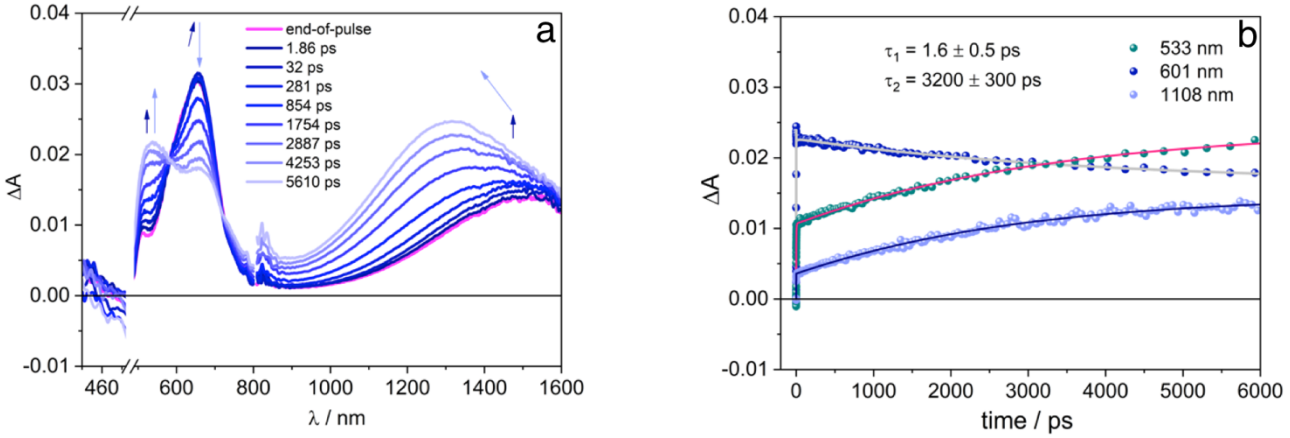

Figure S10. Transient absorption spectra at different delays of **4DPAIPN** in acetonitrile solution containing TBAOx (5.2 mM) (a) and the corresponding ΔA temporal evolutions (and fittings, lines) at significant wavelengths (b). λ_{ex} = 480 nm, A_{480} = 0.18, 0.2 cm optical path, 8 μJ/pulse. In (a) the arrows indicate the spectral changes associated with the different processes.

Transient absorption spectroscopy of the radical anions

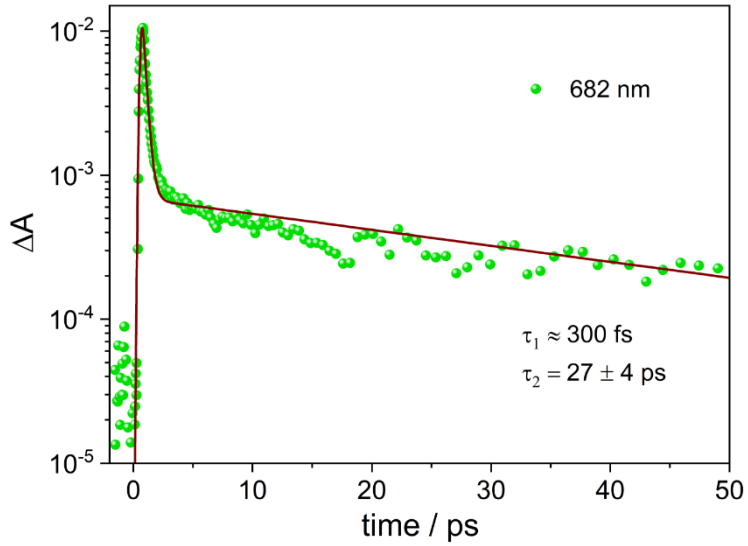

Figure S11. ΔA temporal evolution at 682 nm reported in Figure 3b, main text, represented here in logarithmic scale.

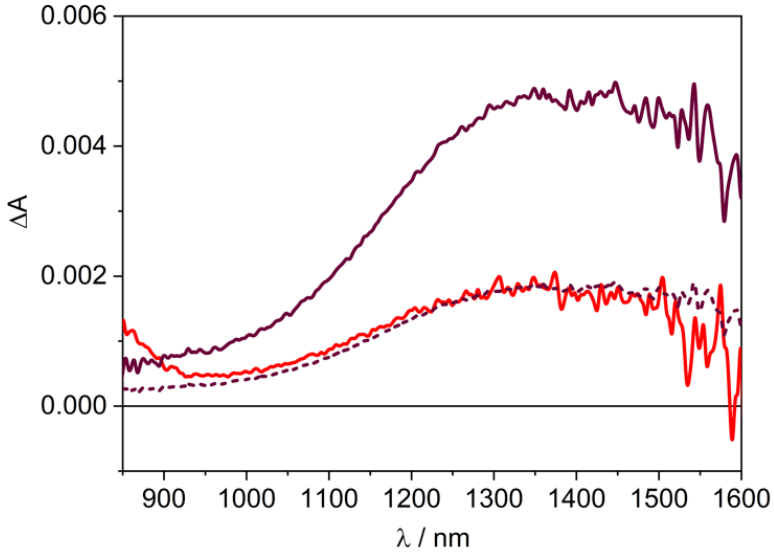

Figure S11. Comparison of the spectrum in the NIR region at 70 ps delay for **4CzIPN**$^{\bullet-}$ (red) and **4DPAIPN**$^{\bullet-}$ (brown, in dashed the normalized spectrum).[6]

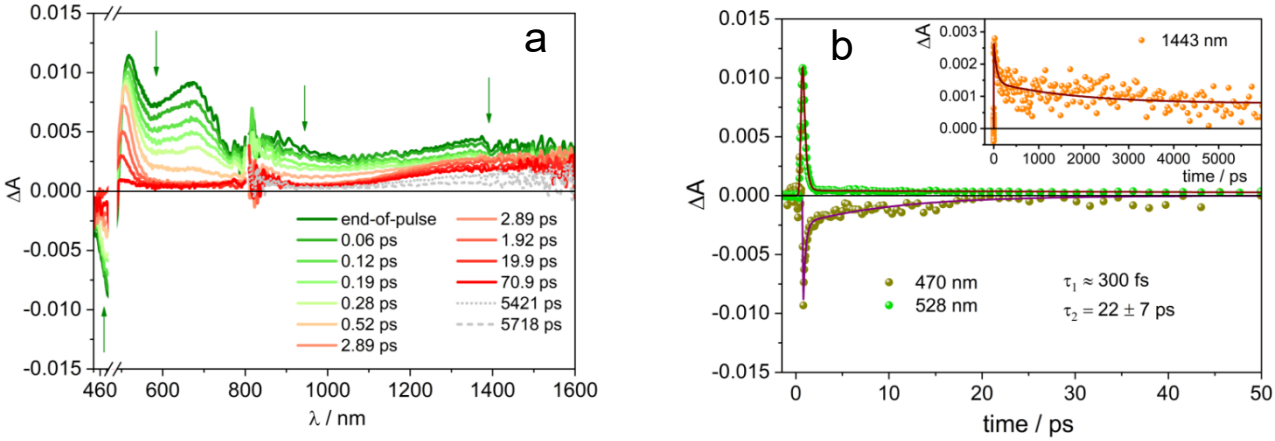

Figure S13. Transient absorption spectra at different delays of a degassed acetonitrile solution of **4CzIPN**$^{\bullet-}$, obtained irradiating a solution of **4CzIPN** and DIPEA (100 mM) at 390 nm (a), and the corresponding ΔA temporal evolution at significant wavelengths (b). λ_{ex} = 480 nm, A_{480} = 0.27, 0.2 cm optical path, 8 μJ/pulse.

Transient absorption spectroscopy of the radical anions with 4-bromoanisole and 4-chloroanisole

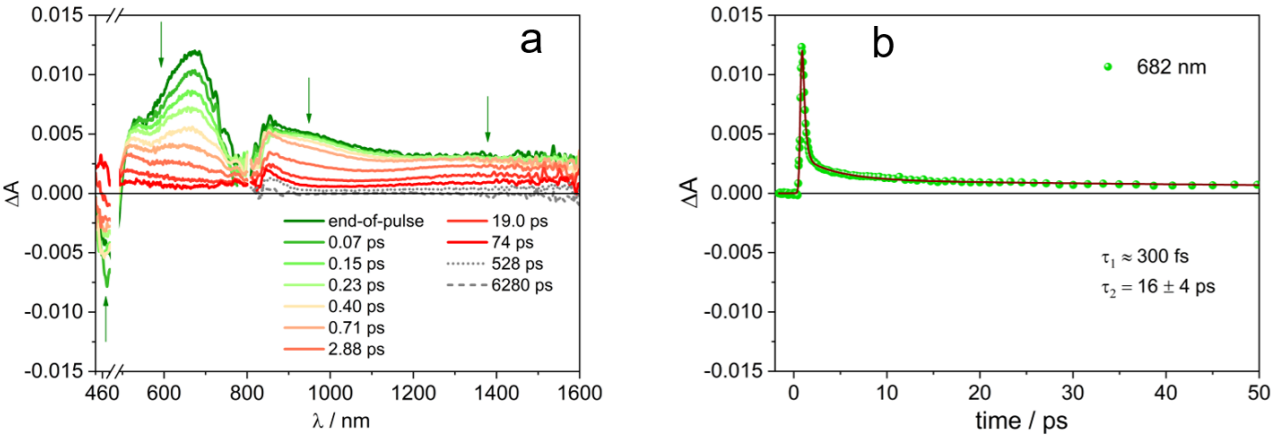

Figure S12. Transient absorption spectra at different delays of a degassed acetonitrile solution of **4CzIPN**$^{\bullet-}$ in the presence of 4-bromoanisole (0.1 M) (a) and the corresponding ΔA temporal evolution at 682 nm (b). λ_{ex} = 480 nm, A_{480} = 0.28, 0.2 cm optical path, 8 μJ/pulse.

The reaction constant for the reduction of 4-bromoanisole by solvated electrons has been derived as the slope of the linear fitting of the plot of Figure 4d, reporting the rate constant of the ΔA decay at 1440 nm as a function of the concentration of 4-bromoanisole (see the figure below for the parameters associated with the fitting). As the decay of the band at 1440 nm is multi-exponential, a weighted average lifetime has been considered to calculate the rate constant at each point (see the table below). At the highest concentration of 4-bromoanisole, the calculated rate constant value is subjected to high uncertainty due to the weakness of the residual band of the solvated electron.

Table S2. Kinetic parameters related to the ΔA decay in the spectral range 1420-1440 nm as a function of the concentration of 4-bromoanisole.

[4-bromoanisole]/M	τ_i[a]/ps	f_i[a,b]	Weighted τ[c]/ps
0	109 2684 4573	0.55 0.15 0.30	1834
0.01	81 2072	0.58 0.42	917
0.1	33 736	0.70 0.30	244

[a] Average values from fittings performed on decays collected at three different wavelengths in the 1420-1440 nm region. [b] Fraction of the pre-exponential factor. [c] Calculated as $\Sigma_i \tau_i f_i$.

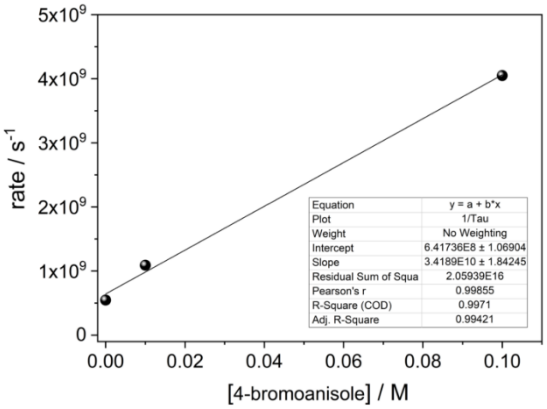

Figure S15. Rate constant of the ΔA decay at 1440 nm as a function of the concentration of 4-bromoanisole and the corresponding fitting parameters of the linear regression.

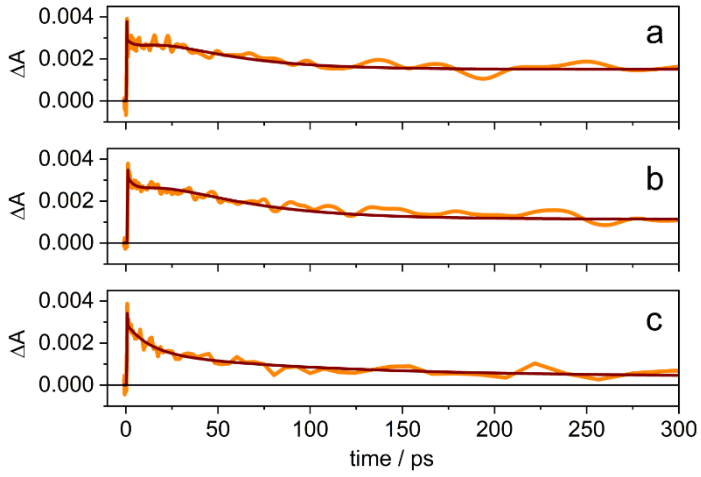

Figure S16. Normalized temporal evolution of ΔA measured at 1440 nm (orange line) for a degassed solution of **4CzIPN**$^{\bullet-}$ (a) and in the presence of 0.01 M (b) and 0.1 M (c) 4-bromoanisole on a shorter time-scale compared to that of Figure 4.

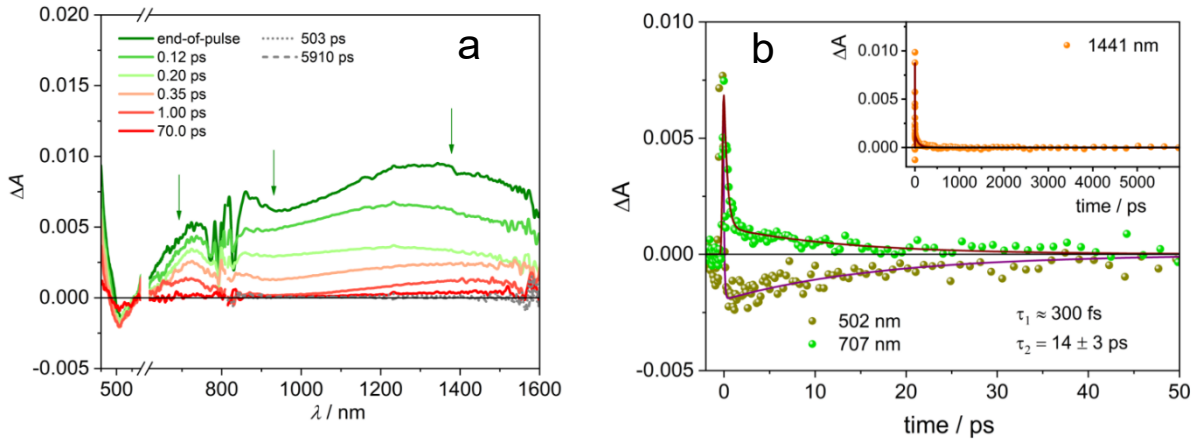

Figure S13. Transient absorption spectra at different delays of a degassed acetonitrile solution of **4DPAIPN**$^{\bullet-}$ in the presence of 4-chloroanisole (0.1 M) (a) and the corresponding ΔA temporal evolution at significant wavelengths (b). λ_{ex} = 600 nm, A_{600} = 0.20, 0.2 cm optical path, 8 μJ/pulse.

The quantum yield of solvated electron production has been estimated as a ratio between the concentration of the produced solvated electron and the concentration of the radical anion excited state, in the excited volume at each laser pulse.

COMPUTATIONAL METHODS

All density functional theory (DFT) and time-dependent DFT (TD-DFT) calculations were carried out using the Gaussian 16A suite of programs adapting a protocol previously used to screen a large number of organic compounds and validated against experimental data.[7,8] Geometry optimizations were carried out at the BLYP35/def2svp level. The corresponding TD-DFT calculations were utilizing the M06-2X/def2svp level of theory on the optimised DFT geometry and optimized first 10 excited states for the calculated absorption spectrum.[9] Solvation effects were all taken into account using acetonitrile based on the polarizable continuum model (PCM).[10] The benchmark of the methodology against 66 dyes gives excellent results (shown in Figure S14) and provides a linear calibration correction to the computed excitation energy which is applied to the results.

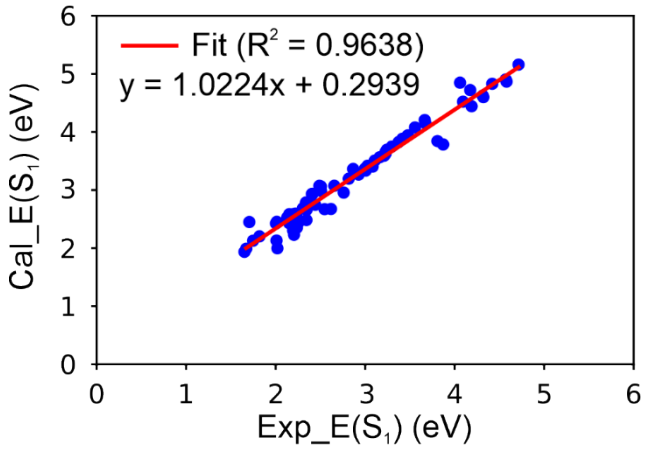

Figure S14. The calibration curve of experimental and computed vertical excitation energy and equation for the calculated absorption spectrum.

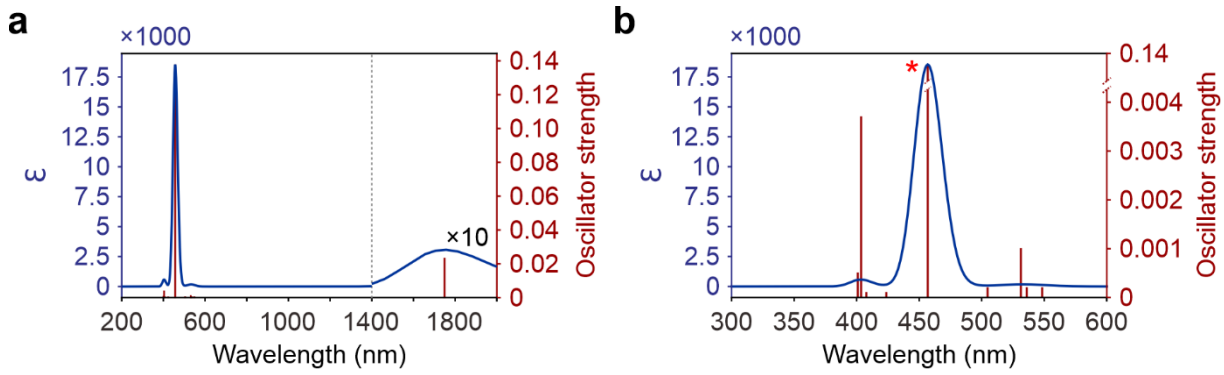

Figure S15. (a) The calculated absorption spectrum of **4CzIPN$^{\bullet-}$** and (b) the corresponding spectrum in the 300nm to 600nm. In (a), the absorption spectrum and oscillator strength are magnified by 10 times in the 1400 - 2000 nm spectral range.

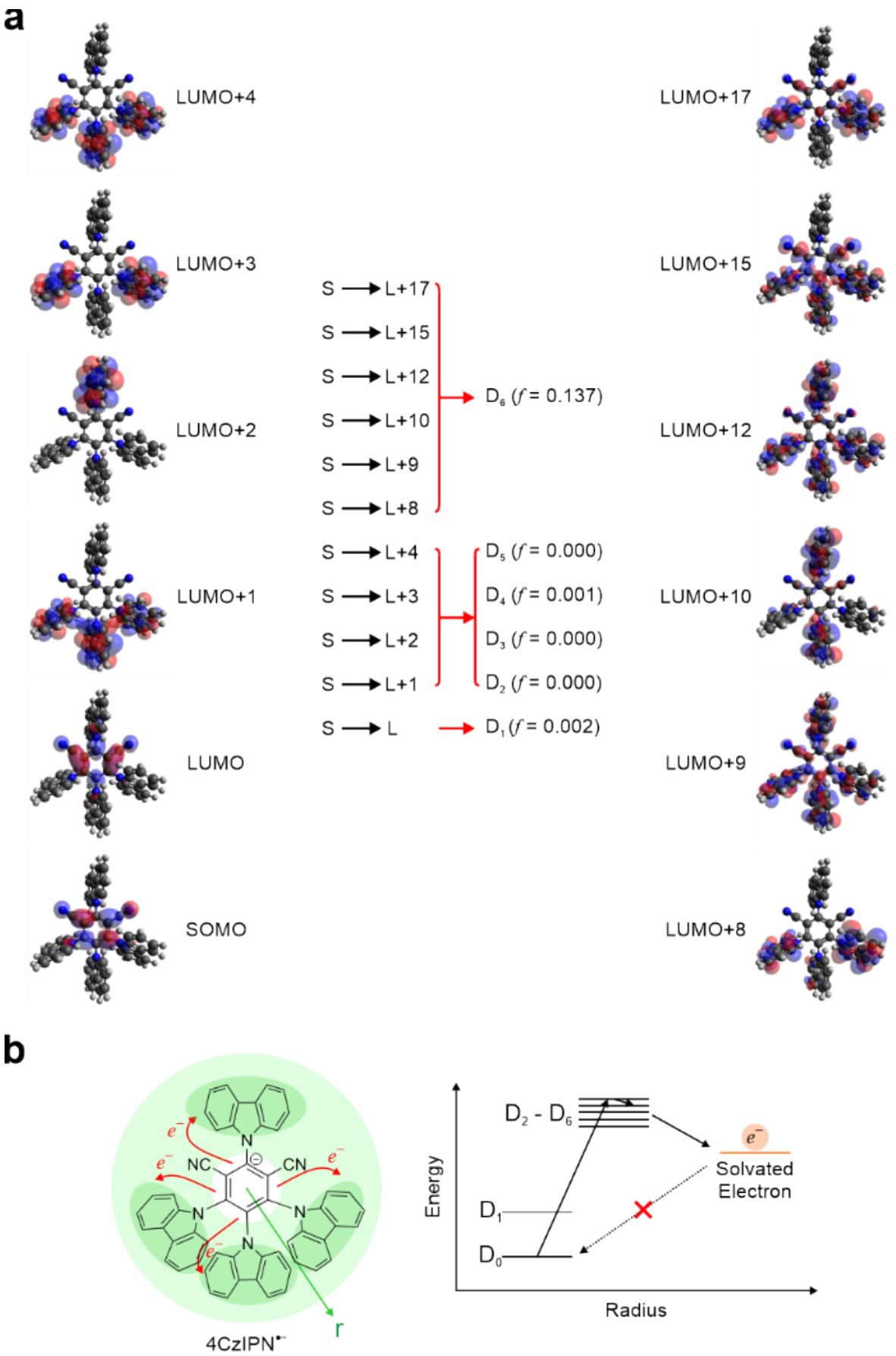

Figure S20. (a) The doublet excited states with oscillator strength of **4CzIPN** and corresponding frontier molecular orbitals. S means the singly occupied molecular orbital (SOMO) and L means the lowest unoccupied molecular orbital (LUMO). (b) The mechanism of **4CzIPN**$^{\bullet-}$ during photophysical processes.

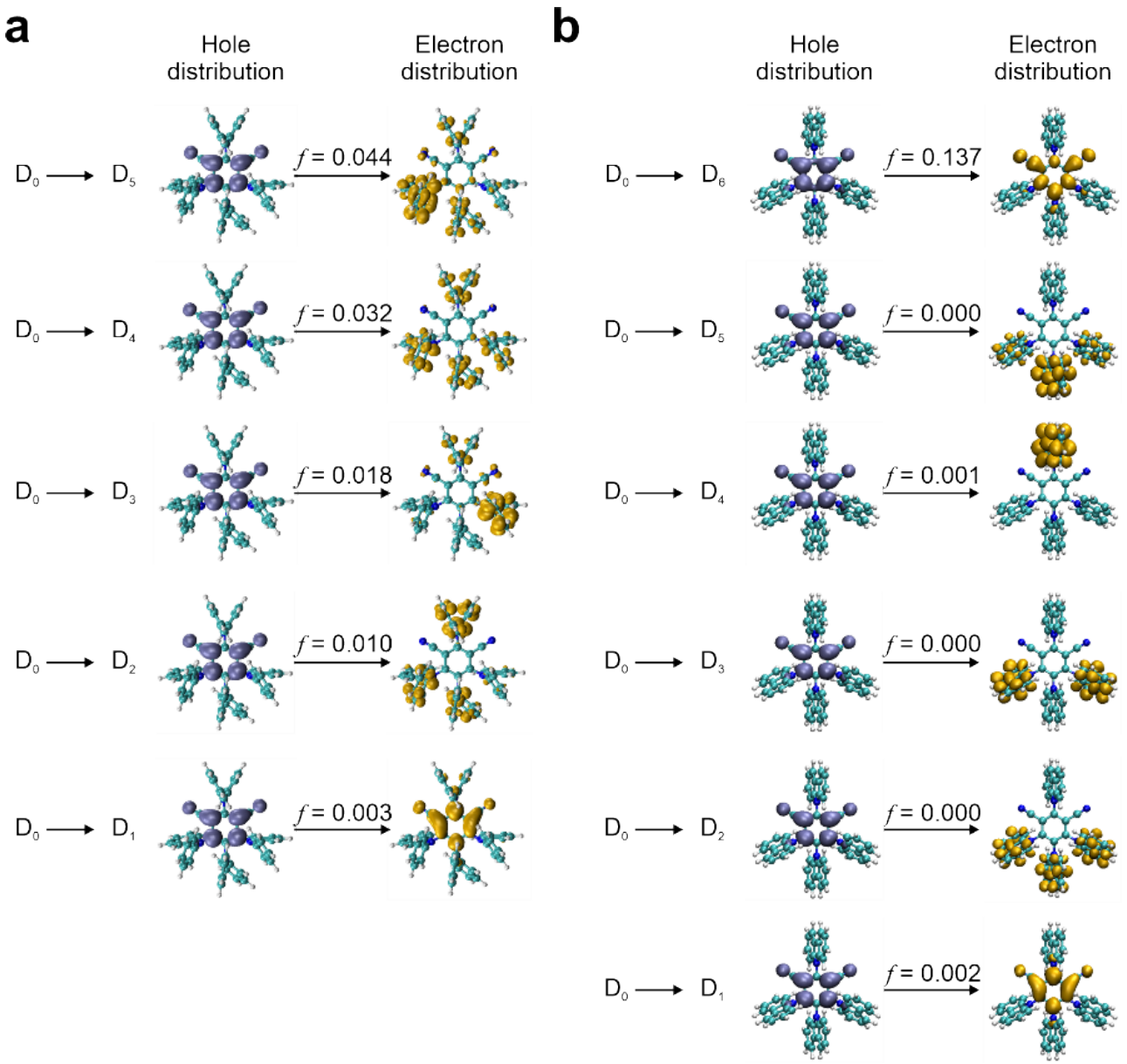

Figure S21. Electron and hole distributions in the different doublet excited states and corresponding oscillator strength in (a) **4DPAIPN**$^{\bullet-}$ and (b) **4CzIPN**$^{\bullet-}$. The hole–electron analysis were investigated by the Multiwfn 3.6.[11]

Supporting Notes and References

(1) Singh, V. K.; Yu, C.; Badgujar, S.; Kim, Y.; Kwon, Y.; Kim, D.; Lee, J.; Akhter, T.; Thangavel, G.; Park, L. S.; Lee, J.; Nandajan, P. C.; Wannemacher, R.; Milián-Medina, B.; Lüer, L.; Kim, K. S.; Gierschner, J.; Kwon, M. S. Highly Efficient Organic Photocatalysts Discovered via a Computer-Aided-Design Strategy for Visible-Light-Driven Atom Transfer Radical Polymerization. *Nat. Catal.* **2018**, *1* (10), 794–804. DOI: 10.1038/s41929-018-0156-8.

(2) Bassan, E.; Inoue, R.; Fabry, D.; Calogero, F.; Potenti, S.; Gualandi, A.; Cozzi, P. G.; Kamogawa, K.; Ceroni, P.; Tamaki, Y.; Ishitani, O. Visible-Light Driven Photocatalytic CO 2 Reduction Promoted by Organic Photosensitizers and a Mn(i) Catalyst. *Sustain. Energy Fuels* **2023**, *7* (14), 3454–3463. DOI: 10.1039/D3SE00546A.

(3) Speckmeier, E.; Fischer, T. G.; Zeitler, K. A Toolbox Approach To Construct Broadly Applicable Metal-Free Catalysts for Photoredox Chemistry: Deliberate Tuning of Redox Potentials and Importance of Halogens in Donor–Acceptor Cyanoarenes. *J. Am. Chem. Soc.* **2018**, *140* (45), 15353–15365. DOI: 10.1021/jacs.8b08933.

(4) Calogero, F.; Potenti, S.; Bassan, E.; Fermi, A.; Gualandi, A.; Monaldi, J.; Dereli, B.; Maity, B.; Cavallo, L.; Ceroni, P.; Cozzi, P. G. Nickel-Mediated Enantioselective Photoredox Allylation of Aldehydes with Visible Light. *Angew. Chem. Int. Ed.* **2022**, *61* (11), e202114981. DOI: 10.1002/anie.202114981.

(5) Beattie, J. W.; White, D. S.; Bheemaraju, A.; Martin, P. D.; Groysman, S. Recyclable Chemosensor for Oxalate Based on Bimetallic Complexes of a Dinucleating Bis(Iminopyridine) Ligand. *Dalt. Trans.* **2014**, *43* (21), 7979–7986. DOI: 10.1039/C4DT00577E.

(6) The residual band at ca. 850 nm in the spectrum of **4CZIPN**$^{\bullet-}$ is likely due to a small fraction of **4CZIPN** excited at 480 nm, since the neutral form has a maximum at this wavelength and a long lifetime of 15 ns.

(7) Frisch, M. J.; Trucks, G. W.; Schlegel, H. B.; Scuseria, G. E.; Robb, M. A.; Cheeseman, J. R.; Scalmani, G.; Barone, V.; Petersson, G. A.; Nakatsuji, H.; Li, X.; Caricato, M.; Marenich, A. V.; Bloino, J.; Janesko, B. G.; Gomperts, R.; Mennucci, B.; Hratchian, H. P.; Ortiz, J. V.; Izmaylov, A. F.; Sonnenberg, J. L.; Williams-Young, D.; Ding, F.; Lipparini, F.; Egidi, F.; Goings, J.; Peng, B.; Petrone, A.; Henderson, T.; Ranasinghe, D.; Zakrzewski, V. G.; Gao, J.; Rega, N.; Zheng, G.; Liang, W.; Hada, M.; Ehara, M.; Toyota, K.; Fukuda, R.; Hasegawa, J.; Ishida, M.; Nakajima, T.; Honda, Y.; Kitao, O.; Nakai, H.; Vreven, T.; Throssell, K.; Montgomery, J. A.; Jr.; Peralta, J. E.; Ogliaro, F.; Bearpark, M. J.; Heyd, J. J.; Brothers, E. N.; Kudin, K. N.; Staroverov, V. N.; Keith, T. A.; Kobayashi, R.; Normand, J.; Raghavachari, K.; Rendell, A. P.; Burant, J. C.; Iyengar, S. S.; Tomasi, J.; Cossi, M.; Millam, J. M.; Klene, M.; Adamo, C.; Cammi, R.; Ochterski, J. W.; Martin, R. L.; Morokuma, K.; Farkas, O.; Foresman, J. B.; Fox, D. J. Gaussian 16, Rev. C.01. *Gaussian 16, Rev. C.*

01 **2016**.

(8) Omar, Ö. H.; Nematiaram, T.; Troisi, A.; Padula, D. Organic Materials Repurposing, a Data Set for Theoretical Predictions of New Applications for Existing Compounds. *Sci. Data* **2022**, *9* (1), 54. DOI: 10.1038/s41597-022-01142-7.

(9) Zhao, Y.; Truhlar, D. G. The M06 Suite of Density Functionals for Main Group Thermochemistry, Thermochemical Kinetics, Noncovalent Interactions, Excited States, and Transition Elements: Two New Functionals and Systematic Testing of Four M06-Class Functionals and 12 Other Function. *Theor. Chem. Acc.* **2008**, *120* (1–3), 215–241. DOI: 10.1007/s00214-007-0310-x.

(10) Tomasi, J.; Mennucci, B.; Cammi, R. Quantum Mechanical Continuum Solvation Models. *Chem. Rev.* **2005**, *105* (8), 2999–3094. DOI: 10.1021/cr9904009.

(11) Lu, T.; Chen, F. Multiwfn: A Multifunctional Wavefunction Analyzer. *J. Comput. Chem.* **2012**, *33* (5), 580–592. DOI: 10.1002/jcc.22885.